Temperature-responsive hybrid nanomaterials based on modified halloysite nanotubes uploaded with silver nanoparticles

Tetiana Shevtsova[1], Giuseppe Cavallaro[2], Giuseppe Lazzara[2], Stefana Milioto[2], Volodymyr Donchak[1], Khrystyna Harhay[1], Sergiy Korolko[3], Andrzej Budkowski[4], Yurij Stetsyshyn[1,4*]

[1]Lviv Polytechnic National University, 12 S. Bandery, 79013 Lviv, Ukraine

[2]Dipartimento di Fisica e Chimica, Università degli Studi di Palermo, Viale delle Scienze pad 17, 90128 Palermo, Italy

[3]Hetman Petro Sahaidachnyi National Army Academy, 32, Heroes of Maidan Street, Lviv 79012 Lviv, Ukraine

[4]Smoluchowski Institute of Physics, Jagiellonian University, Łojasiewicza 11, 30-348 Kraków, Poland

[*]Corresponding authors E-mails: yrstecushun@ukr.net

Graphical abstract

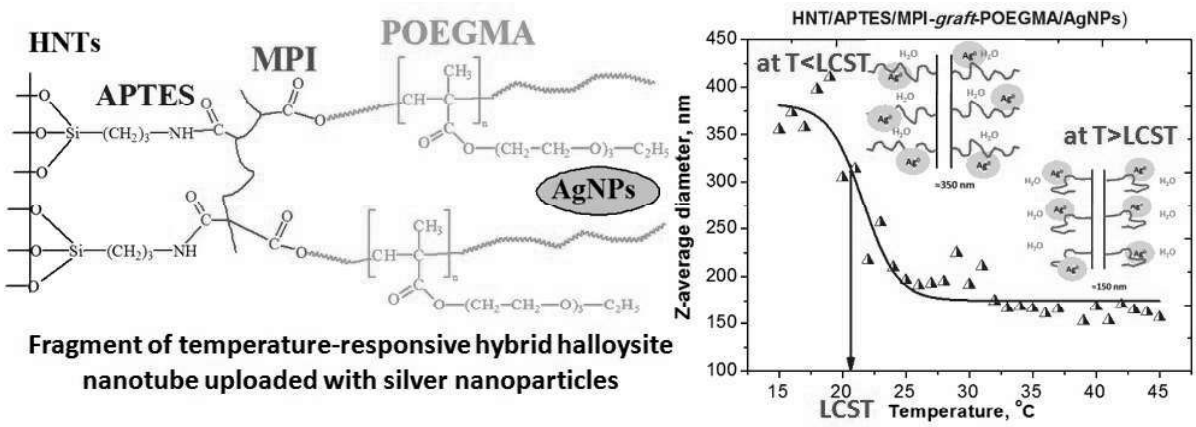

Fragment of temperature-responsive hybrid halloysite nanotube uploaded with silver nanoparticles

KEYWORDS: hybrid nanomaterials; halloysite nanotubes; temperature-responsive polymer brushes; silver nanoparticles.

Abstract

New temperature-responsive hybrid nanomaterials based on modified halloysite nanotubes (HNTs) containing grafted polymer brushes with silver nanoparticles have been successfully fabricated. We used a three steps process including synthesis of the initiating coatings onto HNTs surface, fabrication of the POEGMA - poly(oligo(ethylene glycol)ethyl ether methacrylate) grafted brushes and synthesis of the silver nanoparticles (AgNPs). The synthesis and properties of hybrid nanomaterials were studied by FT-IR, TGA and DLS methods. It is shown that the introduction of AgNPs, formed from 0.005 M $AgNO_3$ solution leads to a significant reduction of low critical solution temperature (LCST) of the polymer layer from 29.7 to 21.6 °C. The samples fabricated from 0.05 M $AgNO_3$ solution did not evidence a temperature-induced transition, despite of the contents of AgNPs obtained for both solutions are almost identical (≈4 %w). The presence of AgNPs with sizes of ca. 20 nm was confirmed in the hybrids prepared from both $AgNO_3$ concentrations by UV-vis spectroscopy, and electron microscopy.

These temperature-responsive hybrid nanomaterials may be used for conservation of solid substrates, production of advanced medical facemasks, photothermal therapy against microorganisms and tumors etc.

1. INTRODUCTION

Nanotubes are nanoscale tube-like structures, which may be synthesized using different type of the chemicals. Now, most famous and prospective are carbon, halloysite, imogolite, boron nitride, silicon, titanium and gallium nitride nanotubes [1]. All kinds of nanotubes possess unique physicochemical and biological properties for their applications in different fields. Modification of the nanotubes is important technological procedure to change their properties in order to reach highly stable dispersions of the nanotubes in water or organic media, to improve their biocompatibility, to insert into the structure of the nanotubes antibacterial or fluorescent components or another substances with special properties [2-3].

Halloysite nanotubes (HNTs) are naturally occurring tubular clay nanomaterials with external diameter of 50−80 nm, made of aluminosilicate kaolin sheets rolled several times. They are a natural nanomaterials with a unique combination of the hollow tubular nanostructures, high aspect ratio, mechanical strength, good dispersibility, wide potential in terms of functionality, biocompatibility, and availability in large quantities at low cost. The aluminol and siloxane groups on the surface of HNT facilitate the formation of hydrogen bonding with the biomaterials onto its surface. HNTs could be additionally modified by various methods, to form both covalent and non-covalent bonds with modifier [4-5]. The outer surface of nanotubes formed by siloxane groups with the presence of some structural defects in the form of -OH groups is appropriate for grafting organosilanes [6-7]. Lazzara's group intensively developed different methods for functionalization of the HNTs by synthetic polymers and biopolymers, silanes and inorganic nanostructures [8-11]. As reported elsewhere [12], HNTs were functionalized by (3-aminopropyl) triethoxysilane (APTES) and then silver nanoparticles (AgNPs) were synthesized through in situ reduction of Ag^{+} ions on their surface. Halloysite nanotubes were extensively employed in different kind of applications, such catalysis [13-19], pharmaceutics [20-26], biomedicine [27-29], cosmetics [30-32], oil/water separation [33] and packaging [34-39].

In our opinion, nowadays, the most promising procedure for functionalization of the nanotube's surface is grafting of polymer brushes by the method of polymerization "from the surface". Successful fabrication of the grafted polymer brushes on surface of nanotubes is non-trivial aim and requires deep knowledge in chemistry of the surface as well as in polymer chemistry [40-43]. In the work [44] magnetic nickel chrysotile nanotubes tailored with poly(methacrylic acid) brushes have been synthesized by surface-initiated atom transfer radical polymerization (SI-ATRP). They were used as a novel canonic nanosorbents for removal of Cu^{2+} ions from aqueous solutions. Polymer brushes on the surface of multiwalled carbon nanotubes

(MWCNTs) were synthesized by grafting 2-hydroxyethyl methacrylate (HEMA) to sidewall of MWCNTs via surface reversible addition and fragmentation chain transfer (RAFT) polymerization [45]. Grafted polyHEMA brushes can be hydrolyzed by HCl solution to yield poly(methacrylic acid) (PMAA) brushes grafted to MWCNTs, which have high loading capacities for metal ions, such as Ag^+. Later they were used for fabrication of MWNT-PMAA/Ag hybrid nanocomposites [45]. A synthetic strategy for the functionalization of HNTs by poly(ethylene glycol)-based brushes via SI-ATRP and following covalent immobilization of penicillin was developed in work [46].

As mentioned above, a special interest was paid to modification of the HNTs. In particular, HNTs were modified with polymer brushes. The modified nanotubes showed high dispersibility in various organic solvents. Amphiphilic brushes of poly(4-vinylpyridine)-block-polystyrene and polystyrene-block-poly(4-vinylpyridine) were grafted onto HNTs via a surface reversible addition-fragmentation chain transfer (RAFT) living polymerization through anchoring R group in RAFT agent S-1-dodecyl-S′-(R,R′-dimethyl-R″-acetic acid) trithiocarbonates [47]. To verify the amphiphilicity of HNTs, with grafted block copolymers, their Pickering emulsification behavior in water/soybean oil diphase mixture was studied.

In our previous works [41-42], we fabricated and studied the stimuli-responsive nanotubes which are able to change their properties as response to external stimuli such as temperature or pH. Stimuli-responsive nanotubes could be useful in numerous biomedical, environmental and analytical applications. Motivated by significant progress in the field of research of nanomaterials based on HNTs we firstly developed the temperature-responsive hybrid nanomaterials based on modified HNTs, uploaded with AgNPs. The first step involved a chemical functionalization of the pristine HNTs via covalent bonding of APTES and following grafting multifunctional peroxide initiator of surface-initiated radical polymerization (MPI) to amino groups of grafted APTES. The second step involved grafting polymerization of the oligo(ethylene glycol)ethyl ether methacrylate - (OEGMA) by the method of initiating “from the surface” of MPI functionalized HNTs. Finally, AgNPs were synthesized using Ag^+ ions adsorbed into the polymer brushes and reduced to AgNPs by sodium borohydride.

The obtained temperature-responsive hybrid nanomaterials were analyzed using thermogravimetric analysis (TGA), Fourier transform infrared spectroscopy (FT-IR) and dynamic light scattering (DLS). Results of TGA and FT-IR analysis demonstrate successful fabrication of the POEGMA brushes. DLS results suggest on well expressed temperature-responsive properties of HNTs functionalized by POEGMA brushes as well as HNTs functionalized by POEGMA brushes with AgNPs. In addition, basing on results of

UV-vis spectroscopy, the presence of AgNPs with sizes of ca. 20 nm was demonstrated. Such materials have attracted considerable interest for many scientists due to their effective antibacterial properties. It shows strong antimicrobial activity and has a broad antibacterial spectrum. We hope that obtained nanomaterial demonstrate both antibacterial and thermo-switchable properties as it was earlier reported in [48-49]. Most promising ways for applications of the temperature-responsive halloysite nanotubes uploaded with AgNPs include the protection and conservation of solid substrates, the production of advanced medical masks, photothermal ablation and radiation-enhanced therapy.

2. EXPERIMENTAL SECTION

2.1. Materials

Pyridine and other organic solvents were purified as reported by Weissberger et al [50]. Poly(ethylene glycol) (PEG-9), pyromellitic dianhidride, PCl_5 were supplied by Merck Chem. Co., OEGMA and APTES – by Sigma-Aldrich. Halloysite nanotubes with a specific surface area of 65 $m^2 \cdot g^{-1}$ and a specific gravity of 2.53 $g \cdot cm^{-3}$ are from Sigma-Aldrich (Milan, Italy).

2.2. Synthesis

2.2.1. Synthesis of tert-butyl hydroperoxide.

tert-Butyl hydroperoxide was obtained as described in [51]. Hydrogen peroxide was alkylated with tert-butyl alcohol in the presence of concentrated sulfuric acid. The fraction boiling in the temperature range of 318-320 K (at 1.6 kPa) was collected. It had the refractive index n_d^{20} = 1.4002 in accord with previous reports (n_d^{20}= 1.4010 [51]).

2.2.2. Synthesis of pyromellitic acid chloride.

Pyromellitic acid chloride was obtained, as described in [52]. In a 500 ml round-bottomed flask equipped with a thermometer and a reflux condenser, connected with water scrubber, 43.6 g (0.2 mol) of pyromellitic dianhydride and 91.6 g (0.44 mol) of PCl_5 were mixed and boiled on the oil bath until the reaction mixture appeared homogeneous. Afterwards, it was additionally mixed for 15-16 h. The temperature of the mixture was kept at 405-408 K. Then, the condenser reflux was replaced by a Liebig condenser and approximately 60-63 g of $POCl_3$ was distilled off during 8 h. Then, the temperature of the mixture increased to 455-458 K. The crude product was then recrystalized from gasoline yielding 51.2 g (78.1 %) of a colorless crystalline product with the melting point 340 K (in accord with literature value 341 K [52]); Acid number AN = 1373 mg KOH/g (calculated value is 1368 mg KOH/g).

2.2.3. Synthesis of MPI with residual acid chloride groups.

MPI with residual acid chloride groups was synthesized as described in [53]. 4.6 g (0.014 mol) of pyromellitic acid chloride was dissolved in 15 ml of anhydrous dichlorethane, placed in three-necked flask, equipped with stirrer, and 1.26 g (0.014 mol) of tert-butylhydroperoxide was added. The mixture was cooled down to 278 K, and, then, 1.1 g (0.014 mol) of pyridine dissolved in 10 ml of anhydrous dichlorethane, was added dropwise at 278 K. Subsequently, the suspension was mixed for 1 hour. THE, 5.6 g (0.014 mol) of PEG-9 was added, and again the solution of 2.2 g (0.028 mol) pyridine in 10 ml of anhydrous dichlorethane was admixed dropwise. The mixture was then stirred for another 3 hours, and the temperature rised gradually up to 288-293 K. The precipitate of pyridinium chloride was filtered out. The solvent was distilled out and the pellet was dried in vacuum (100-200 Pa) at 313 K for 3 h, yielding 8.2 g (81 %) of oligoperoxide. The pellet had a yellowish resin-like appearance. Its characteristics are summarized as follows: content of active oxygen - 1.9 % (calc. 2.2 %); content of active chlorine - 5.4 % (calc. 4.9 %); AN=163.1 mg KOH/g (calculated value is 155.3 mg KOH/g); IR-spectra showed chararcteristic bands of ν(C=O) in Ar-C(O)Cl, ν(C=O) in ester group at 1760 and 1752 sm^{-1}; doublet at 1390, 1365 sm^{-1}, referred to d($C(CH_3)_3$) and a band of tert-butoxy group at 848 sm^{-1}. The chemical structure of the MPI is presented in Fig. 1.

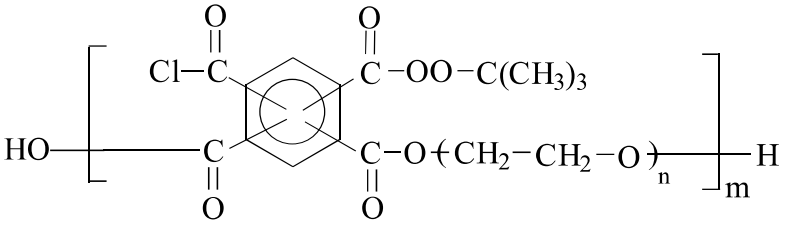

Figure 1. The chemical structure of the MPI, n = 9; m = 3÷5.

2.3. Modification of HNTs

2.3.1. Modification of HNTs with APTES.

0.5 mL of APTES was dissolved in 25 mL of mixture methanol and water (90/10). Approximately 0.5 g of clay powder was added, and the suspension was dispersed ultrasonically for 20 min. Then it was stirred at 70 °C for 4 h. The solid phase was filtered out, washed six times with toluene to remove the excess of APTES and dried overnight at 70 °C yielding 0.45 g of APTES modified HNTs.

2.3.2. Modification of APTES modified HNTs with MPI.

50 mg of APTES modified HNTs powder was mixed with 50 ml of MPI solution in anhydrous dioxane (1 mg/ml) and sonicated for 20 min. Afterwards, the solution was stirred vigorously for 24

h. The excess of MPI was removed by dispersing with sonication in dioxane and than in toluene. The purified HNTs with grafted MPI were centrifuged, dried and used for grafting of POEGMA.

2.3.3. Fabrication of POEGMA grafted brushes. HNTs with grafted MPI were placed in a container with 0.1 M OEGMA aqueous solution and sonicated for 20 min. Then, the mixture was stirred and heated under argon atmosphere at 90 °C for a 48 h, resulting in the POEGMA-*graft*-MPI functionalized HNTs. They were purified by dispersing with sonication in ethanol or water, and centrifuged. The purified POEGMA-graft-MPI functionalized HNTs were dried and stored as a powder.

2.3.4. Fabrication of the AgNPs.

POEGMA-graft-MPI functionalized HNTs were dipped in aqueous 0.05 or 0.005 M $AgNO_3$ solutions, sonicated for 5 minutes and stirred for 25 min under argon flow. Then adsorbed silver ions were reduced to form AgNPs by 0.2 M $NaBH_4$ solution for 12 h. Thereafter, the functionalized HNTs were removed from solution by centrifugation, washed several times with distilled water and dried under argon.

2.4. Characterization of HNTs

2.4.1. Thermogravimetric Analysis (TGA). TGA analyses were performed using a Perkin Elmer Pyris 1 TGA instrument, Thermal Analysis Gas Station and Pyris Version 11.1.1.0497 software. The samples were analyzed under N_2 gas flow, from 30.00 to 600.00 °C using a heating rate of 10 °C/min.

2.4.2. Fourier transform infrared spectroscopy (FT-IR). FT-IR spectra were recorded on NICOLET iS50 FT-IR spectrometer (Thermo Scientific, USA), equipped with iS50 ATR multi-range, diamond sampling station. The sample powders were either placed on diamond crystal or mixed with KBr to form a pellet. The spectra in range 4000-350 cm^{-1} with a 5 cm^{-1} step were collected in reflection or in transmission mode.

2.4.3. Dynamic light scattering (DLS). The size distribution and zeta potential measurements of the nanotubes were performed with a Zetasizer Nano ZS (Malvern, USA) at 25°C. The Nano ZS contains a 4-mW He-Ne laser operating at a wavelength of 633 nm and an avalanche photodiode detector. The scattered light was detected at an angle of 173°. The refractive index and absorption of the nanomaterial were assumed to be 2.0 and 1.500, respectively. All size and zeta potential measurements were carried out in triplicate. All data were analysed by using the Malvern instrument DST 5.00 software. The 1 mg of samples were suspended in 1 mL distilled water and sonicated for

2-10 min. After the sonication, low speed (1000 g, 5 min, 25°C) centrifugation was carried out and the supernatant (Figure 1) was used for analysis.

2.4.4 UV-vis spectroscopy. UV-vis spectra were registered by a Specord S600 Analytik Jena UV-Vis spectrophotometer on aqueous dispersions of POEGMA-*graft*-MPI functionalized HNTs containing AgNPs. The concentration of the dispersions was fixed at 0.01 wt%. The experiments were conducted at 25 °C using quartz cuvettes.

2.4.5 TEM. For transmission electron microscopy (TEM), the Jeol JEM 2100 microscope was used. The acceleration voltage was set at 200 kV. A drop of the aqueous dispersion of POEGMA-*graft*-MPI functionalized HNTs containing AgNPs was deposited in a 3 mm nickel grid holey carbon coated (Taab) and solvent evaporated under ambient conditions.

3. RESULTS AND DISCUSSION

Novel temperature-responsive hybrid nanomaterials based on modified halloysite nanotubes uploaded with AgNPs were fabricated in three steps process: synthesis of the initiating coatings onto HNTs surface; fabrication of the POEGMA grafted brushes and synthesis of the AgNPs (see Schema 1). The first step involved chemical functionalization of the "native" HNTs (**1**) via covalent bonding of APTES (**2**) and following grafting MPI (**3**) to amino groups of the attached APTES taking advantage of the interaction between amino groups of APTES coatings and pyromellitic chloroanhydride fragments in MPI molecules. The second step involved the grafting polymerization of the oligo(ethylene glycol)ethyl ether methacrylate (OEGMA) (**4**) initiated "from the surface" of MPI functionalized HNTs. Finally, Ag^+ ions were adsorbed into the POEGMA brushes due to strong affinity of oxygen in ether groups of the POEGMA with silver ions and reduced to metallic Ag (**5**) by sodium borohydride. Successful synthesis of the metallic nanoparticles strongly depends on location and amount of the ligands in polymer motifs. A strong affinity of silver ions with poly(4-vinylpyridine), poly(1-vinyl-1,2,4-triazole), POEGMA or poly(hydroxyethyl methacrylate) as well as 2-(N-dodecylbenzimidazol-2′-yl)-6-(N-{[(4-ethynylphenyl)oxy]dodecyl}benzimidazol-2′-yl)pyridine functionalized poly(ethylene glycol)s with K_2PtCl_4 was described in [48-49, 54-57]. The functionalization process and properties of modified HNTs were studied by FT-IR and UV-vis spectroscopies, TGA and DLS methods.

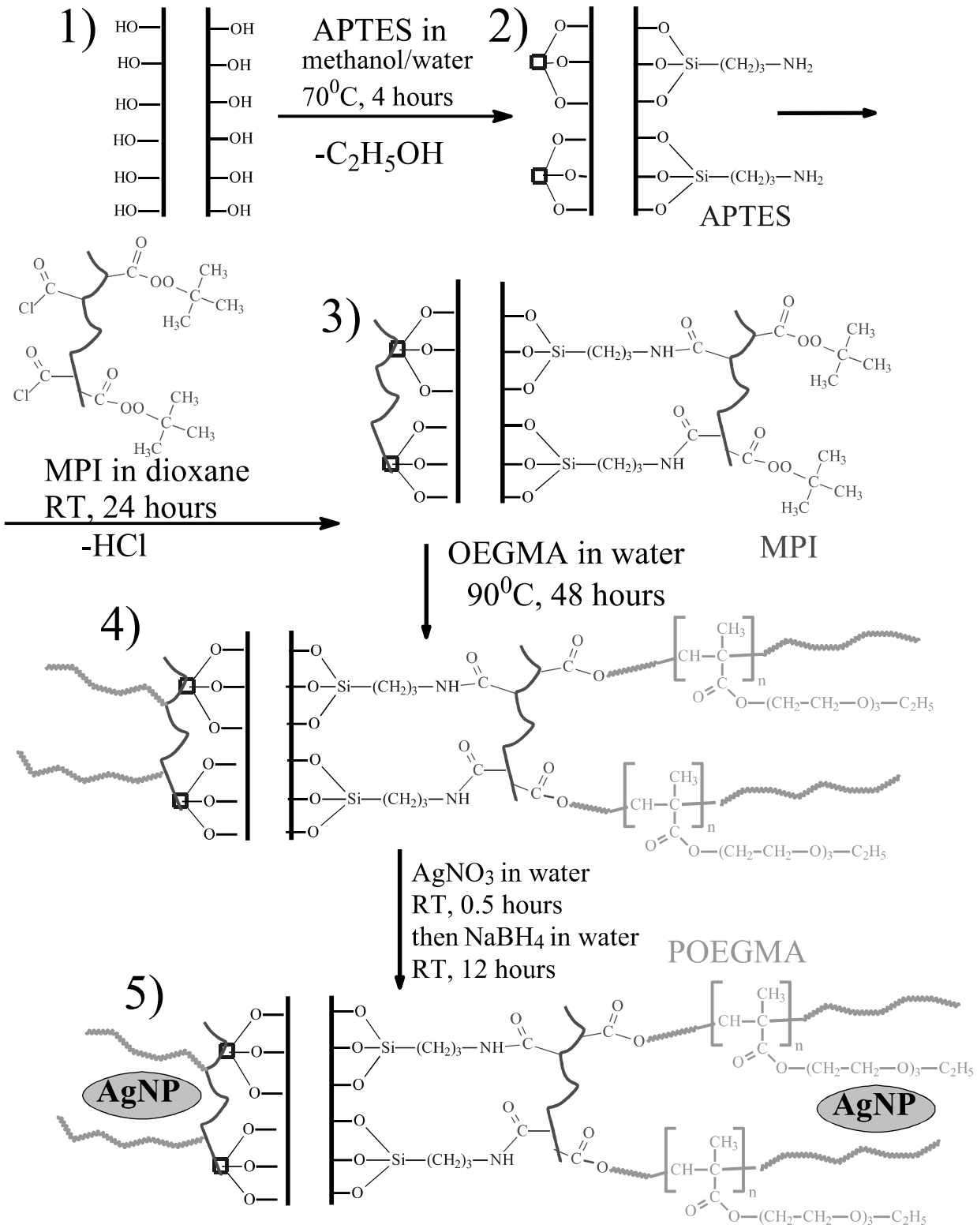

Scheme 1. Chemical functionalization of "native" HNTs (1) with APTES (2) and following grafting MPI (see structure in Fig.1) to amino groups of grafted APTES (3), subsequent grafting copolymerization of OEGMA, initiated by peroxide groups of MPI (4) resulting in POEGMA functionalized HNTs (5) which are uploaded with AgNPs (5).

3.1. Fabrication and properties of the temperature-responsive halloysite nanotubes

FTIR spectra of native HNTs, APTES and APTES/MPI-*graft*-POEGMA functionalized HNTs are displayed in Fig.2 and interprated in Table 1.

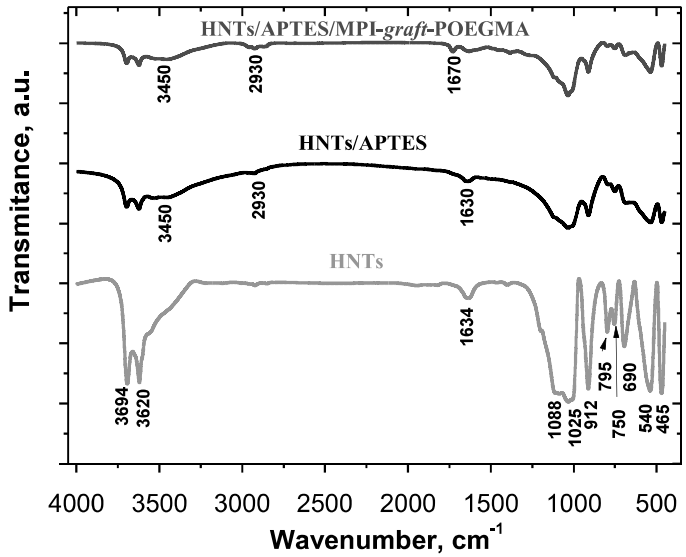

Figure 2. Fourier transforms infrared spectra of HNT (green line), HNT/APTES (black line) and HNT/APTES/MPI-graft-POEGMA (red line)

Table 1.

Some absorption frequencies at FTIR spectra of „native“ HNTs, HNTs modified with APTES and APTES/MPI-*graft*-POEGMA modified HNTs

Samples	Wavenumber (cm^{-1})										
	v (O–H)	*v* (H_2O)	*v* (NH_2)	*v* (CH_2)	*v* (C=O)	*v* (Si–O) in-plane	*δ* (O–H)	*v* (Si–O) sym.	*v* (Si–O) perp.	*δ* (Si–O–Al)	*δ* (Si–O–Si)
„native“ HNT	3694 3620					1088 1025	912	795	750 690	540	465
HNT/APTES	3694 3620	3450	3360	2930		1088 1025	912	795	750 690	540	465
HNT/APTES /MPI-*graft*-POEGMA	3694 3620	3450		2930	1670	1088 1025	912			540	465

The frequency and assignment of each vibrational mode observed for unmodified and modified HNTs are based on previous reports [6] and completely confirm the modification process. Specific bands at 3694 cm^{-1} and 3620 cm^{-1} are assigned to O-H stretching of inner hydroxy groups of HNTs (green colour). Bands at 912 cm^{-1} – to O-H deformation of inner hydroxyl groups, at 1088 and 1025 cm^{-1} – to in-plane Si-O stretching, at

795 cm^{-1} – to symmetric stretching of Si-O, at 750 cm^{-1} and 690 cm^{-1} – to perpendicular Si-O stretching, at 540 cm^{-1} – to deformation of Al-O-Si and at 465 cm^{-1} – to deformation of Si-O-Si bonds.

After modification with APTES (black color) intensities of the picks assigned to characteristic groups of the HNTs became essentially lower. The broad peak of water OH stretch, at 3450 cm^{-1}, is more centered and well expressed in the spectra of HNTs functionalized with APTES, which is attributed to the overlap with the $-NH_2$ stretching vibration signal around 3360 cm^{-1}. Appeared a new band at 2930 cm^{-1} assigned to the stretching of CH_2 fragments. Absence of majority APTES bands at HNTs/APTES spectrum is related with a small amount of APTES at the HNTs surface (4-5 %). Absence of majority of bands of APTES molecules in HNTs/APTES spectrum is related with small amount of APTES at the HNTs surface (4-5 %). The spectrum of HNT/APTES/MPI-*graft*-POEGMA (red color) is similar to this one of HNT/APTES. The difference is in emergence of the low but very well expressed band of carbonyl stretching at 1670 cm^{-1} and increasing of intensity of the band CH_2 stretching at 2930 cm^{-1}. In general, the basic patterns of change of spectra in the process of modification differ insignificantly from those described in details in our previous publications [41-42].

Fig. 3 shows the TG curves for HNT, HNT/APTES, and HNT/APTES/MPI-graft-POEGMA samples. All thermograms (Fig.3) demonstrate a slight weight loss at a temperatures of about 50-120°C, connected with dehydration of physically adsorbed water [58-61]. Second stage of the degradation of "native" HNTs are in interval within 110°C and 460°C due to decomposition of structural water or bound water [58-61] (Fig.3, green). Significant weight loss of HNTs starts at 460°C and ends approximately at 600°C. This range is specific for HNTs and it is related to dehydroxylation of the structural aluminol groups (Al–OH) [6]. The total weight loss for HNTs is nearly 15%.

TG curve of HNT/APTES (Fig.3, black) showed three degradation steps. The first weight loss was observed between 120-250 °C and, probably, it is attributed to degradation of hydrogen-bonded APTES existing in the cross-linking framework [6]. They are much less thermally stable than the covalently bonded APTES, and decompose at a lower temperature. The second temperature range of weight loss is between 250 and 450°C. This step is associated to several stages of thermal decomposition including decomposition of the APTES species grafted onto SiOH and AlOH groups on the edges or external surface, the oligomerized APTES, and the APTES grafted on AlOH groups at the internal surface of the lumen [6]. The third step

occurred between 450 and 515°C. The total weight loss for HNT/APTES is nearly 20% suggesting that nearly 4.6 wt.% is related to degradation of the APTES.

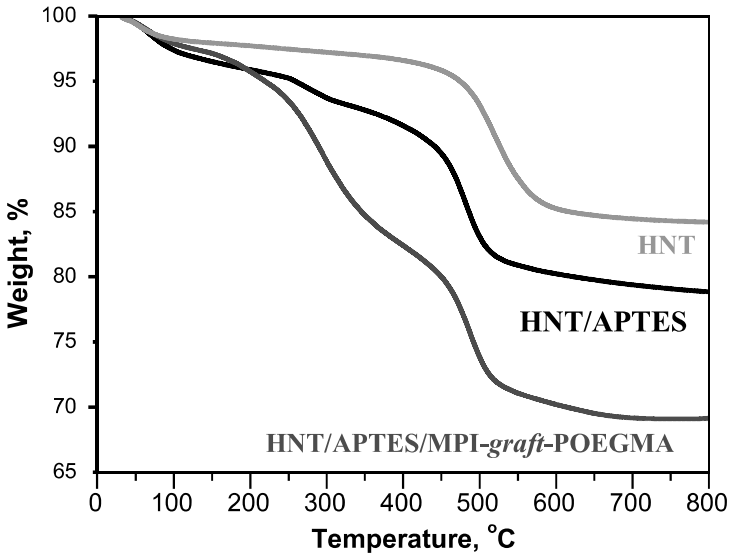

Figure 3. TG curves of HNT, HNT/APTES and HNT/APTES/MPI-graft-POEGMA

In contrast to previous curves, curve attributed to HNT/APTES/MPI-graft-POEGMA strongly loses weight demonstrating gradual destruction, ending about at 530 °C. The decomposition of different fragments of HNT/APTES/MPI-graft-POEGMA is partially overlapped, making a complex multistep loses weight and the boundary between different processes cannot be accurately defined. The range between 180 and 450 °C indicates the weight loss due to decomposition of APTES/MPI as well as POEGMA molecules. The next range, which starts from 450 °C, is similar to the HNTs and HNT/APTES thermogravimetric curves. The total weight loss for HNT/APTES/MPI-graft-POEGMA is ≈31%. The difference between the weight loss of HNT/APTES/MPI-graft-POEGMA and HNT/APTES is 12.6% and corresponds to MPI-graft-POEGMA quantity on the HNTs surface.

Figure 4 demonstrates the distribution curve of the hydrodynamic diameter of HNT/APTES/MPI-graft-POEGMA, measured in the temperature range from 15 to 45°C. Samples with grafted POEGMA brushes show a well-defined and reproducible response to temperature with LCST at 29.7±0.7 °C, which is in good agreement with data published in other studies [54]. Temperature-sensitive grafted polymer brushes are ultrathin polymer coatings consisting of polymer chains that are tethered with one chain end to an interface, which generally is a solid substrate [51]. They have unique ability to change their physico-chemical properties reversibly in relatively small temperature intervals [54]. Temperature-responsive properties of the

POEGMA grafted brushes are explained by the formation of hydrogen bonds between ether oxygens of poly(ethylene glycol) and water hydrogens at T<LCST. This balance is disrupted at T>LCST, where polymer-polymer interactions are thermodynamically favored in comparison to polymer-water interactions [54, 62-65].

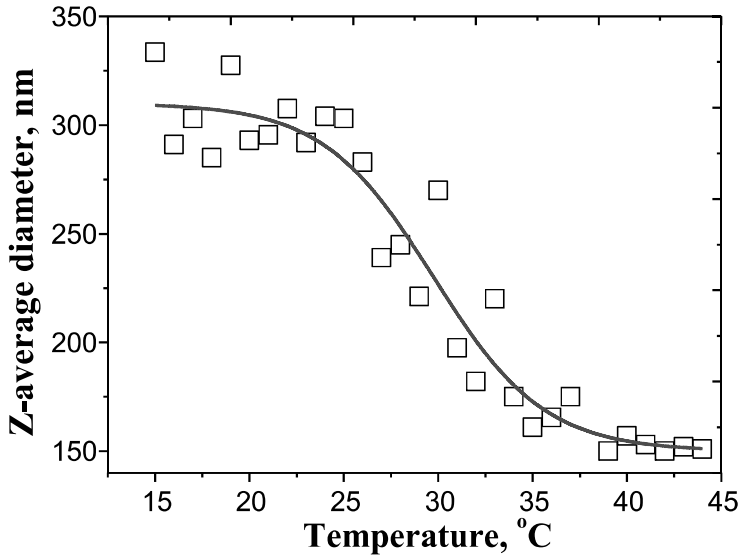

Figure 4. Impact of temperature on the Z-average hydrodynamic diameter of HNT/APTES/MPI-*graft*-POEGMA.

This causes the transition of grafted polymer chains from the conformation of stretched hydrated brushes to the conformation of collapsed hydrophobic chains, which coagulate and lead to a decrease in the average hydrodynamic diameter HNT/APTES/MPI-*graft*-POEGMA with grafted brushes (figure 5).

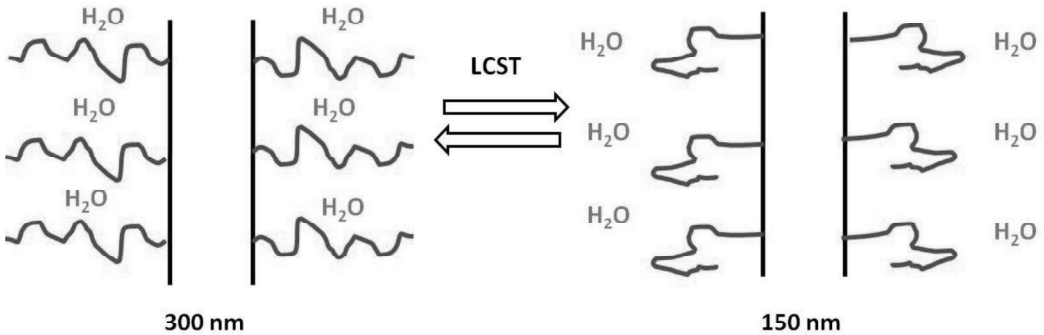

Figure 5. Temperature-induced change of the Z-average hydrodynamic diameter of HNT/APTES/MPI-*graft*-POEGMA

3.2. Fabrication and properties of temperature-responsive halloysite nanotubes uploaded with AgNPs

In our previous works [48-49, 66] we have fabricated and characterized in details temperature-responsive antibacterial coatings based on grafted polymer brushes with embedded AgNPs. For this, Ag^+ ions were adsorbed into the polymer coatings and reduced to metallic silver in the form of nanoparticles. As reducing agent a sodium borohydride was used.

In turn to previous results, HNT/APTES/MPI-graft-POEGMA were dipped in 0.05 or 0.005 M $AgNO_3$ aqueous solutions and then adsorbed silver ions were reduced to AgNPs by sodium borohydride. TGA curves of the HNT/APTES/MPI-graft-POEGMA and HNT/APTES/MPI-graft-POEGMA with AgNPs obtained from 0.05 or 0.005 M $AgNO_3$ solutions are presented in Fig.6. All curves are similar at temperatures lower 450 °C, but after this value, the appearance of the curves differs significantly. We observe essentially reduced weight loss for samples with AgNPs in comparison to „native" HNT/APTES/MPI-graft-POEGMA. The HNT/APTES/MPI-graft-POEGMA demonstrates ≈31% weight loss, in contrary to another two samples with AgNPs which lost only 27% of weight. This indicates that content of the organic phase in the samples with AgNPs is lower than in „native" HNT/APTES/MPI-graft-POEGMA and confirms fabrication of the AgNPs on the surface of nanotubes.

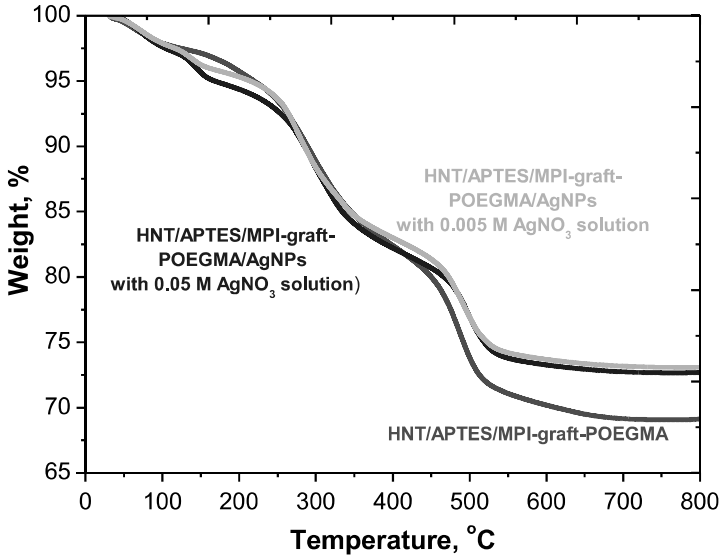

Figure 6. TGA of the HNT/APTES/MPI-graft-POEGMA, HNT/APTES/MPI-graft-POEGMA with AgNPs obtained from 0.05 or 0.005 M $AgNO_3$ solutions

In Table 2 the values of weight loss at 800 °C for HNT/APTES/MPI-graft-POEGMA and samples with AgNPs as well as contents of AgNPs are presented. Calculated contents of the AgNPs in both samples are nearly 4%.

Table 2.

The weight loss values at 800 °C for HNT/APTES/MPI-graft-POEGMA and these ones with AgNPs

Sample	Weight loss, %	AgNPs, %
HNT/APTES/MPI-graft-POEGMA	30.9	0
HNT/APTES/MPI-graft-POEGMA/AgNPs with 0,005 M $AgNO_3$ solution	27.3	3.6
HNT/APTES/MPI-graft-POEGMA/AgNPs with 0,05 M $AgNO_3$ solution	26.9	4.0

The effect of temperature on the hydrodynamic diameter of HNT/APTES/MPI-graft-POEGMA and HNT/APTES/MPI-graft-POEGMA/AgNPs fabricated from 0.05 or 0.005 M $AgNO_3$ solutions is presented in Figure 6. HNT/APTES/MPI-graft-POEGMA and HNT/APTES/MPI-graft-POEGMA/AgNPs fabricated from 0.05 or 0.005 M $AgNO_3$ solutions represent different behaviors within the studied temperature range (15 to 45°C).

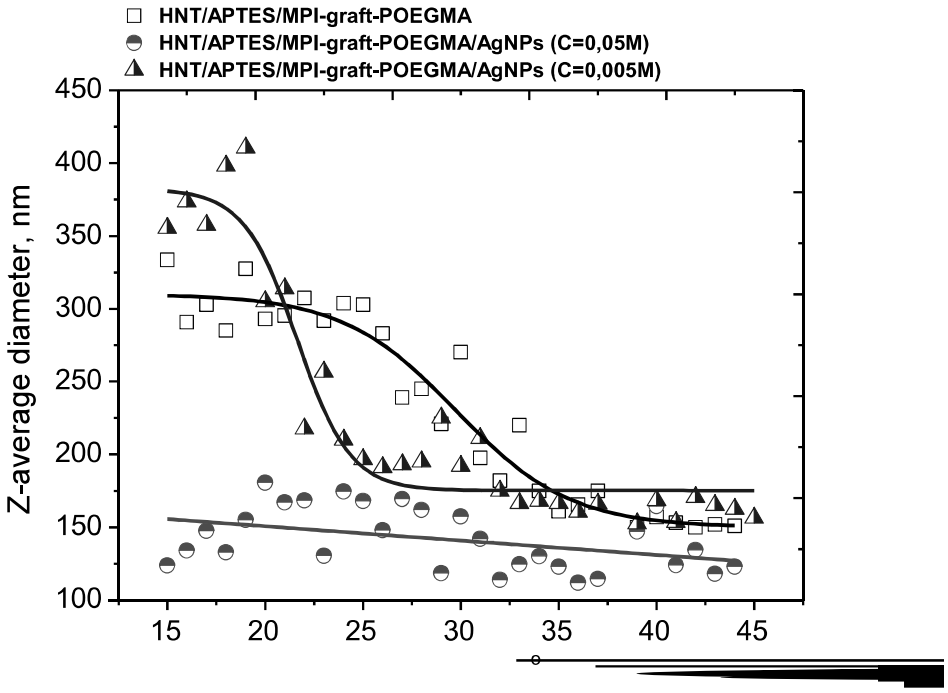

Figure 7. Impact of the temperature on the Z-average hydrodynamic diameter of the HNT/APTES/MPI-graft-POEGMA and HNT/APTES/MPI-graft-POEGMA/AgNPs fabricated from C=0.05 or 0.005 $AgNO_3$ solutions.

Dependences of the hydrodynamic radius from temperature for HNT/APTES/MPI-graft-POEGMA and HNT/APTES/MPI-graft-POEGMA/AgNPs fabricated from 0.005 $AgNO_3$ solution demonstrate similar trends fitting by Boltzmann's curve. Their hydrodynamic diameters decrease from 350 up to 160 nm at LCST. As

was reminded above LCST for HNT/APTES/MPI-graft-POEGMA was equal 29.7±0.7 °C. The same analysis (Fig. 7.), for HNT/APTES/MPI-graft-POEGMA/AgNPs fabricated from 0.005 $AgNO_3$ solution showed the LCST nearly 21.6±0.5 °C suggesting on essential impact of the AgNPs on LCST. In contrast, the average diameter of HNT/APTES/MPI-graft-POEGMA/AgNPs fabricated from 0.05M $AgNO_3$ solution is almost constant at about 150 nm for studied temperature range suggesting on absence of temperature-sensitive properties. Similar results were described in work [48] where strong dependence between concentration of the embedded AgNPs and temperature-responsive properties of POEGMA grafted brush coatings was demonstrated. The content of the AgNPs obtained for samples which were synthesized from solutions with different $AgNO_3$ concentrations are almost identical (≈4 % wt), but in one case the temperature-responsive properties are blocked and in another one a very well expressed temperature-induced changes were demonstrated. It seems that not only concentration of the AgNPs has strong impact on temperature-responsive properties but also manner of the fabrication and their morphology does so. Probably, AgNPs fabricated from 0.05M $AgNO_3$ solution create dense shell around the POEGMA coatings blocking temperature-responsive properties. At the same time, for samples fabricated from 0.005M $AgNO_3$ solution AgNPs are uniformly distributed in POEGMA coatings. Hypothetical scheme of the temperature-induced change of the hydrodynamic radius of HNT/APTES/MPI-graft-POEGMA/AgNPs fabricated from 0.005M $AgNO_3$ solution are depicted in Figure 8.

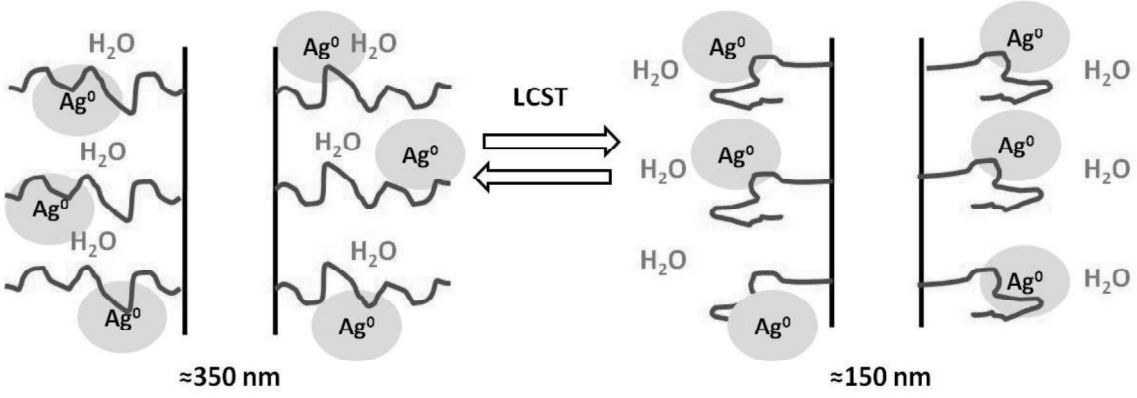

Figure 8. Temperature-induced change of the Z-average hydrodynamic diameter of HNT/APTES/MPI-graft-POEGMA/AgNPs fabricated from 0.005M $AgNO_3$ solution.

The presence of AgNPs within the structure of POEGMA functionalized HNTs was demonstrated by UV-vis spectroscopy. As shown in Figure 9, the spectra of HNT/APTES/MPI-graft-POEGMA/AgNPs evidended a broader absoprtion signal (in the wavelenght range between ca. 370 and 440 nm) that can be attributed to

colloidal AgNPs [67-68]. This observation is valid for HNT/APTES/MPI-graft-POEGMA/AgNPs fabricated from $AgNO_3$ solution with different concentration (0.05 and 0.005 M). We determined the Ag conduction band energy form the cut off wavelength of the absorption peaks. Based on the corresponding condution band energy (3.039 eV) and related literature [68], we calculated that both samples present AgNPs of ca. 20 nm. The HNT/APTES/MPI-graft-POEGMA/AgNPs composite was also imaged by TEM and the nanotubular morphology was evidenced with a clear coating layer that contains also particles with higher contrast as expected for AgNPs (Figure 9) that possess a size compatible with UV-VIS findings.

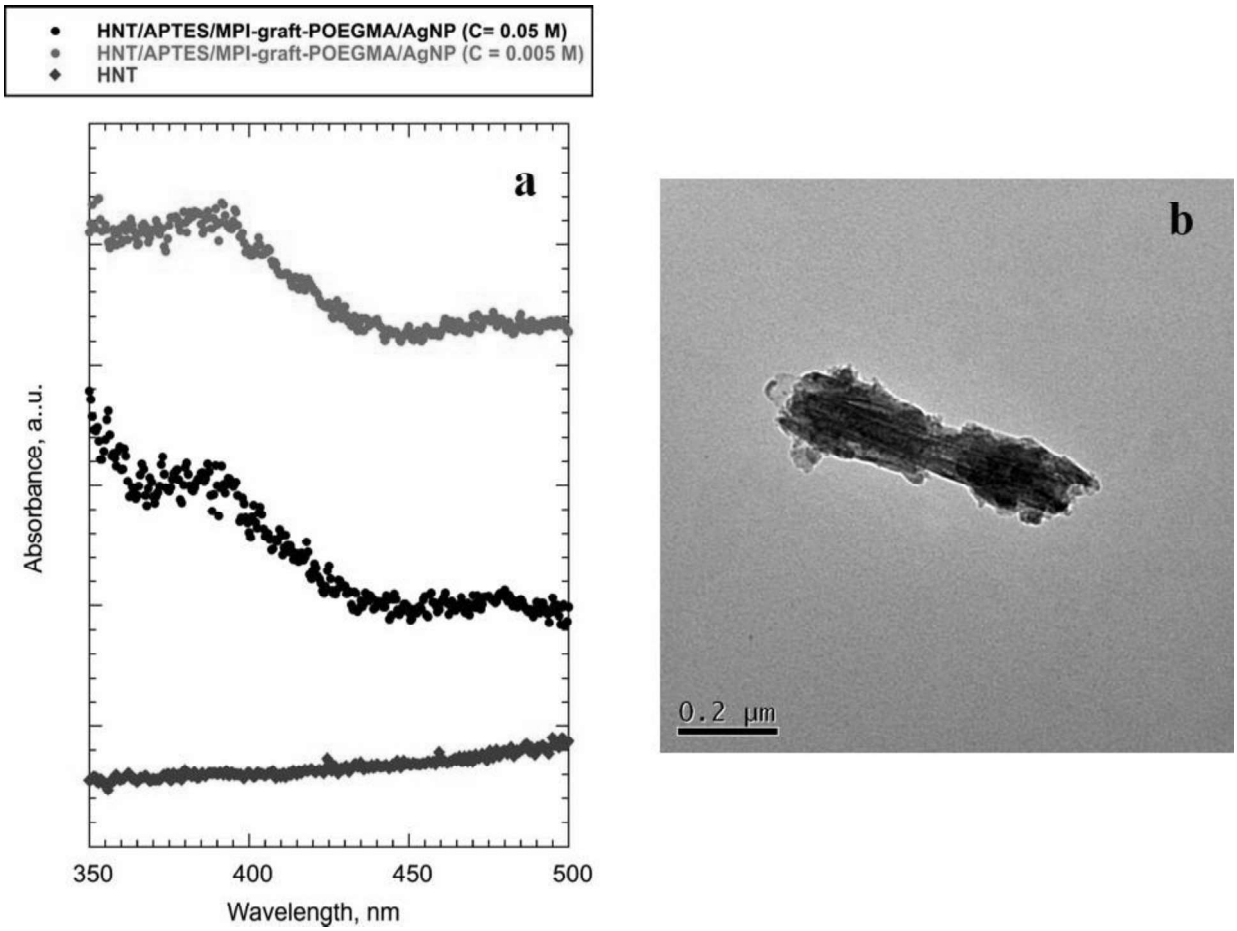

Figure 9. (a) UV-vis absorption spectra for HNT and HNT/APTES/MPI-graft-POEGMA/AgNPs fabricated from C=0.05 or 0.005 $AgNO_3$ solutions. (b) TEM image for HNT/APTES/MPI-graft-POEGMA/AgNPs fabricated from C=0.05 M $AgNO_3$.

3.3. Possible ways for applications of the temperature-responsive halloysite nanotubes uploaded with AgNPs

Within past years, application of the AgNPs has become a popular trend in scientific works. It is interesting to compare use of combination of words “silver” and “nano” in Scopus for last 30 years. As it can

be seen from Table 3 this combination has not been in use in 1990, but the number of remarks grew intensively during last 30 years.

Table 3.

Statistics of remarks for combination of the words “silver” and “nano” in Scopus for last 30 years

Year	Amount of the remarks
1990	0
2000	38
2010	985
2020	1143

First of all this interest is related to diminution in efficiency of current biocides and antibiotics, leading to increased mortality and higher medical costs. On the other hand, fundamentally new approaches towards usage of the AgNPs were proposed. For example, a hyperthermic treatment caused by the photo-thermal effect of the AgNPs under near-infrared laser irradiation can induce localized hyperthermia, which is used to kill bacteria or cancer cells [69-70]. Another example it are “smart” coatings which are able simultaneously to kill bacteria and to self-clean the surface from killed ones [48-49, 71-72]. And last prominent work [73] what we would like to mention here is fabrication of microorganisms coated with AgNPs, so-called "cyborgs", that are capable of delivering nanoparticles to living organisms.

Our previous experience in area of the hybrid nanomaterials with AgNPs [48-49] and analysis of the literature sources allow to propose four most promising ways for applications of the temperature-responsive halloysite nanotubes uploaded with AgNPs. These reflections are presented in Fig.10. One of them is the potential use for surface protection and conservation of solid substrates (marble, stone, glass, bronze, and bread-made artifacts) [74]. As was demonstrated earlier [75-79] polymer/nanoclay hybrids are efficient protective agents for coating and surface cleaning of artwork. Thin protective layer of the temperature-responsive halloysite nanotubes uploaded with AgNPs deposited on solid substrates is a promising agent for long-term protection against bacteria and fungi.

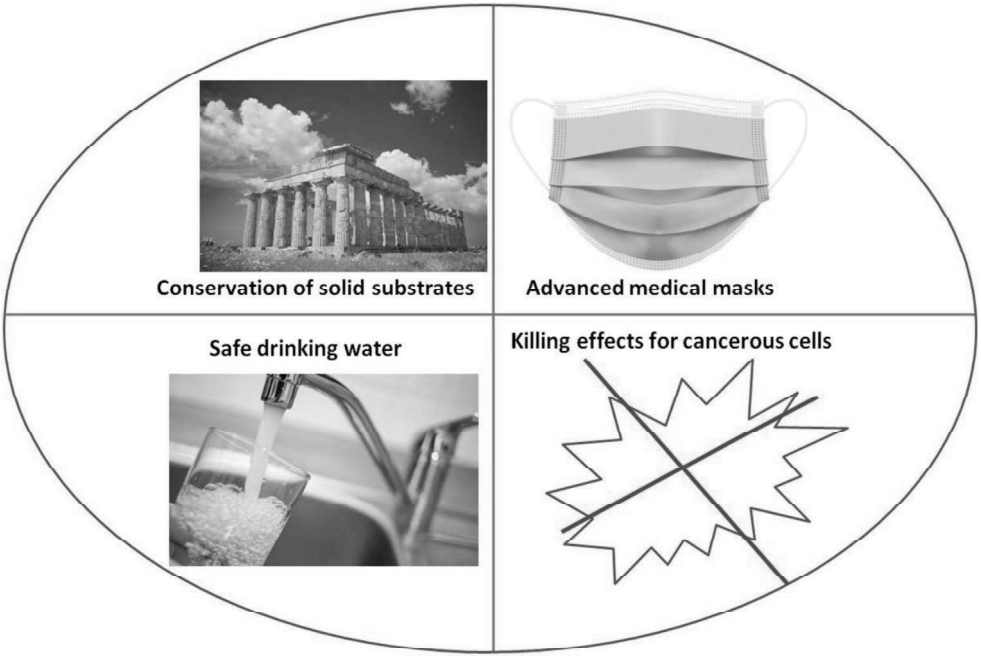

Figure 10. Most promising ways for applications of the temperature-responsive halloysite nanotubes uploaded with AgNPs

Second way is connected with usage of the temperature-responsive halloysite nanotubes uploaded with AgNPs for production of advanced medical masks. Masks might prevent the virus transmission and protect people especially vulnerable to infection by being a physical barrier to the droplets [80]. This is a very actual task developed in last two years because of COVID-19 pandemic. It has recently been shown [80-81] that facemasks fabricated with polymer composition materials including the metal nanoparticles have antiviral effect against SARS-CoV-2. This effect can be essentially enhanced using near-infrared laser irradiation causing photo-thermal phenomenon to allow reusable application of the facemasks.

Third, application of the temperature-responsive halloysite nanotubes uploaded with AgNPs to obtain safe drinking water. In the work [82] the thermosensitive POEGMA gels were obtained and used as an adsorbents with ability to adsorb oil, adjusting the adsorption activity depending on the temperature of the water. On the other hand, bacteria, fungi and viruses in water can be destroyed using two mechanisms based on silver ions release and photo-thermal effect [83-84].

And finally, temperature-responsive halloysite nanotubes uploaded with AgNPs may be used for photothermal ablation or radiation-enhanced therapy. As it was described in the work [85], a nanoparticles consisting of silver nanoshell with a carbon core were synthesized and killing effects for cancerous cells of each therapeutic modality was demonstrated.

Conclusions

Novel temperature-responsive hybrid nanomaterials based on modified halloysite nanotubes uploaded with AgNPs were successfully fabricated in three-step process (synthesis of the initiating coatings onto HNTs surface, fabrication of the POEGMA grafted brushes and synthesis of the AgNPs). Obtained hybrid materials have some distinct advantages. First, they demonstrate responsive properties reversibly switching solubility and hydrodynamic radius as a response to small changes in temperature. Second, they are uploaded with AgNPs which essentially broads the potency of their applications, especially for killing of microorganisms or cancerous cells. Third, POEGMA modified halloysite nanotubes uploaded with AgNPs probably are biocompatible, nontoxic, nonimmunogenic, demonstrate antifouling/stealth behavior and could be easy uptaken by cells.

The functionalizion and properties of modified HNTs were studied by FT-IR, TGA and DLS. In contrast to POEGMA modified HNTs with LCST at 29.7±0.7 °C, samples uploaded with AgNPs fabricated from 0.005 M $AgNO_3$ solution showed the LCST nearly 21.6±0.5 °C suggesting on essential impact of the AgNPs on LCST. The samples of HNT/APTES/MPI-graft-POEGMA/AgNPs fabricated from 0.05 M $AgNO_3$ solution had no temperature-induced transitions. Meanwhile the contents of the AgNPs in both samples are almost identical (≈4 %w) suggesting that not only concentration of AgNPs has strong impact on temperature-responsive properties but also manner of their fabrication and morphology. Based on the analysis of UV-vis spectra, we demonstrated the presence of AgNPs within the HNT/APTES/MPI-graft-POEGMA structures. From the calculated condution band energy (3.039 eV), we determined that the fabrication of the hybrid nanomaterials using $AgNO_3$ solutions with variable concentration (0.05 and 0.005 M) induced the formation of AgNPs (sizes of ca. 20 nm).

Obtained temperature-responsive hybrid nanomaterials based on modified halloysite nanotubes uploaded with AgNPs have at least four most promising ways for applications which will be developed in our following works (for surface protection and conservation of solid substrates; for production of advanced medical facemasks; for obtaining safe drinking water; for photothermal therapy against microorganisms and tumors).

References

1. M. Serra, R. Arenal, R. Tenne, An overview of the recent advances in inorganic nanotubes, Nanoscale 11 (2019) 8073-8090. https://doi.org/10.1039/C9NR01880H.

2. A.M. Díez-Pascual, Chemical Functionalization of Carbon Nanotubes with Polymers: A Brief Overview, Macromol. 1 (2021) 64-83. https://doi.org/10.3390/macromol1020006.

3. J. Goldberger, R. Fan, P. Yang, Inorganic nanotubes: a novel platform for nanofluidics, Acc. Chem. Res. 39 (2006) 239-248. https://doi.org/10.1021/ar040274h.

4. Y. Yang, Y. Chen, F. Leng, L. Huang, Z. Wang, W. Tian, 2017. Recent advances on surface modification of halloysite nanotubes for multifunctional applications. Appl. Sci. 7, 1215. https://doi.org/10.3390/app7121215.

5. M.J. Saif, H.M. Asif, M. Naveed, Properties and modification methods of halloysite nanotubes: a state-of-the-art review, J. Chil. Chem. Soc. 63 (2018) 4109-4125.

6. P. Yuan, P.D. Southon, Z. Liu, M.E. Green, J.M. Hook, S.J. Antill, C.J. Kepert, Functionalization of halloysite clay nanotubes by grafting with γ-aminopropyltriethoxysilane, J. Phys. Chem. C, 112 (2008) 15742-15751. https://doi.org/10.1021/jp805657t.

7. P. Sun, G. Liu, D. Lv, X. Dong, J. Wu, D. Wang, Effective activation of halloysite nanotubes by piranha solution for amine modification via silane coupling chemistry, RSC Adv. 5 (2015) 52916-52925. https://doi.org/10.1039/C5RA04444H.

8. S. Batasheva, M. Kryuchkova, R. Fakhrullin, G. Cavallaro, G. Lazzara, F. Akhatova, L. Nigamatzyanova, V. Evtugyn, E. Rozhina, R. Fakhrullin, 2020. Facile fabrication of natural polyelectrolyte-nanoclay composites: Halloysite nanotubes, nucleotides and DNA study. Molecules 25, 3557. https://doi.org/10.3390/molecules25153557.

9. G. Infurna, G. Cavallaro, G. Lazzara, S. Milioto, N.T. Dintcheva, 2021. Understanding the effects of crosslinking and reinforcement agents on the performance and durability of biopolymer films for cultural heritage protection. Molecules 26, 3468. https://doi.org/10.3390/molecules26113468.

10. F. Parisi, F. Bernardini, G. Cavallaro, L. Mancini, S. Milioto, D. Prokop. Halloysite nanotubes/pluronic nanocomposites for water logged archeological wood: thermal stability and X-ray microtomography, J. Therm. Anal. Calorim. 141 (2020) 981-989. https://doi.org/10.1007/s10973-020-09637-4.

11. M. Massaro, M. Casiello, L. D'Accolti, G. Lazzara, AngeloNacci, G, Nicotra, R. Noto, A. Pettignano, C. Spinella, S. Riela, 2020. One-pot synthesis of ZnO nanoparticles supported on halloysite nanotubes for catalytic applications. Appl. Clay Sci. 189, 105527. https://doi.org/10.1016/j.clay.2020.105527.

12. S. Kumar-Krishnan, A. Hernandez-Rangel, U. Pal, O. Ceballos-Sanchez, F.J. Flores-Ruiz, E. Prokhorov, O. Arias de Fuentes, R. Esparza, M. Meyyappan, Surface functionalized halloysite nanotubes decorated with silver nanoparticles for enzyme immobilization and biosensing, J. Mater. Chem. B 4 (2016) 2553-2560. https://doi.org/10.1039/C6TB00051G.

13. Y. Liu, J. Zhang, H. Guan, Y. Zhao, J.H. Yang, B. Zhang, Preparation of bimetallic Cu-Co nanocatalysts on poly (diallyldimethylammonium chloride) functionalized halloysite nanotubes for hydrolytic dehydrogenation of ammonia borane, Appl. Surf. Sci. 427 (2018) 106-113. https://doi.org/10.1016/j.apsusc.2017.08.171.

14. Y. Feng, X. Zhou, J.H. Yang, X. Gao, L. Yin, Y. Zhao, B. Zhang, Encapsulation of ammonia borane in Pd/halloysite nanotubes for efficient thermal dehydrogenation, ACS Sustain. Chem. Eng. 8 (2020) 2122-2129. https://doi.org/10.1021/acssuschemeng.9b04480.

15. S. Sadjadi, M. Malmir, M.M. Heravi, F.G. Kahangi, Biocompatible starch-halloysite hybrid: An efficient support for immobilizing Pd species and developing a heterogeneous catalyst for ligand and copper free coupling reactions, Inter. J. Biol. Macromol. 118 (2018) 1903-1911. https://doi.org/10.1016/j.ijbiomac.2018.07.053.

16. S. Sadjadi, M.M. Heravi, S.S. Kazemi, Ionic liquid decorated chitosan hybridized with clay: A novel support for immobilizing Pd nanoparticles, Carbohydr. Polym. 200 (2018) 183-190. https://doi.org/10.1016/j.carbpol.2018.07.093.

17. Y. Zhao, W. Kong, Z. Jin, Y. Fu, W. Wang, Y. Zhang, B. Zang, Storing solar energy within Ag-Paraffin@Halloysite microspheres as a novel self-heating catalyst, Appl. Energy 222 (2018) 180-188. https://doi.org/10.1016/j.apenergy.2018.04.013.

18. L. Lisuzzo, G. Cavallaro, S. Milioto, G. Lazzara, Halloysite nanotubes as nanoreactors for heterogeneous micellar catalysis, J. Colloid Interf. Sci. 608 (2022) 424-434. https://doi.org/10.1016/j.jcis.2021.09.146.

19. A. Glotov, A. Vutolkina, A. Pimerzin, V. Vinokurov, Y. Lvov, Clay nanotube-metal core/shell catalysts for hydroprocesses, Chem. Soc. Rev. 50 (2021) 9240-9277. https://doi.org/10.1039/D1CS00502B.

20. B. Wang, Z. Han, B. Song, L. Yu, Z. Ma, H. Xu, M. Qiao, 2021. Effective drug delivery system based on hydrophobin and halloysite clay nanotubes for sustained release of doxorubicin. Colloids Surf. A Physicochem. Eng. Asp. 628, 127351. https://doi.org/10.1016/j.colsurfa.2021.127351.

21. C. Cheng, Y. Gao, W. Song, Q. Zhao, H. Zhang, H. Zhang, 2020. Halloysite nanotube-based H_2O_2-responsive drug delivery system with a turn on effect on fluorescence for real-time monitoring. Chem. Eng. J. 380, 122474. https://doi.org/10.1016/j.cej.2019.122474.

22. F. Liu, L. Bai, H. Zhang, H. Song, L. Hu, Y. Wu, X. Ba, Smart H_2O_2-responsive drug delivery system made by halloysite nanotubes and carbohydrate polymers, ACS Appl. Mater. Interfaces 9 (2017) 31626-31633. https://doi.org/10.1021/acsami.7b10867.

23. P. Dramou, M. Fizir, A. Taleb, A. Itatahine, N.S. Dahiru, Y.A. Mehdi, H. He, Folic acid-conjugated chitosan oligosaccharide-magnetic halloysite nanotubes as a delivery system for camptothecin, Carbohydr. Polym. 197 (2018) 117-127. https://doi.org/10.1016/j.carbpol.2018.05.071.

24. A.C. Santos, C. Ferreira, F. Veiga, A.J. Ribeiro, A. Panchal, Y. Lvov, A. Agarwal, Halloysite clay nanotubes for life sciences applications: From drug encapsulation to bioscaffold, Adv. Colloid Interface Sci. 257 (2018) 58-70. https://doi.org/10.1016/j.cis.2018.05.007.

25. L. Lisuzzo, G. Cavallaro, P. Pasbakhsh, S. Milioto, G. Lazzara, Why does vacuum drive to the loading of halloysite nanotubes? The key role of water confinement, J. Colloid Interface Sci. 547 (2019) 361-369. https://doi.org/10.1016/j.jcis.2019.04.012.

26. L. Lisuzzo, G. Cavallaro, S. Milioto, G. Lazzara, Halloysite nanotubes filled with salicylic acid and sodium diclofenac: effects of vacuum pumping on loading and release properties, J. Nanostruct. Chem. 11 (2021) 663-673. https://doi.org/10.1007/s40097-021-00391-z.

27. S. Kouser, A. Prabhu, K. Prashantha, G.K. Nagaraja, J.N. D'souza, K.M. Navada, D.J. Manasa, 2022. Modified halloysite nanotubes with Chitosan incorporated PVA/PVP bionanocomposite films: Thermal, mechanical properties and biocompatibility for tissue engineering. Colloids Surf. A Physicochem. Eng. Asp. 634, 127941. https://doi.org/10.1016/j.colsurfa.2021.127941.

28. M. Liu, R. Fakhrullin, A. Novikov, A. Panchal, Y. Lvov, 2019. Tubule nanoclay-organic heterostructures for biomedical applications. Macromol. Biosci. 19, 1800419. https://doi.org/10.1002/mabi.201800419.

29. J. Liao, S. Peng, M. Long, Y. Zhang, H. Yang, Y. Zhang, J. Huang, 2020. Nano-Bio interactions of clay nanotubes with colon cancer cells. Colloids Surf. A Physicochem. Eng. Asp. 586, 124242. https://doi.org/10.1016/j.colsurfa.2019.124242.

30. G. Cavallaro, S. Milioto, S. Konnova, G. Fakhrullina, F. Akhatova, G. Lazzara, Y. Lvov, Halloysite/keratin nanocomposite for human hair photoprotection coating, ACS Appl. Mater. Interfaces, 12 (2020) 24348-24362. https://doi.org/10.1021/acsami.0c05252.

31. A.C. Santos, A. Panchal, N. Rahman, M. Pereira-Silva, I. Pereira, F. Veiga, Y. Lvov, 2019. Evolution of hair treatment and care: Prospects of nanotube-based formulations. Nanomaterials 9, 903. https://doi.org/10.3390/nano9060903.

32. A. Panchal, G. Fakhrullina, R. Fakhrullin, Y. Lvov, Self-assembly of clay nanotubes on hair surface for medical and cosmetic formulations. Nanoscale 10 (2018) 18205-18216. https://doi.org/10.1039/C8NR05949G.

33. P. Cai, K. Di, J. Lv, S. Li, X. Chen, 2021. Environmentally benign and durable superhydrophobic coatings based on short fluorocarbon chain siloxane modified halloysite nanotubes for oil/water separation. Colloids Surf. A Physicochem. Eng. Asp. 630, 127540. https://doi.org/10.1016/j.colsurfa.2021.127540.

34. G. Gorrasi, V. Bugatti, G. Viscusi, V. Vittoria, Physical and barrier properties of chemically modified pectin with polycaprolactone through an environmentally friendly process, Colloid Polym. Sci. 299 (2021), 429-437. https://doi.org/10.1007/s00396-020-04699-0.

35. M. Barman, S. Mahmood, R. Augustine, A. Hasan, S. Thomas, K. Ghosal, Natural halloysite nanotubes/chitosan based bio-nanocomposite for delivering norfloxacin, an anti-microbial agent in sustained release manner, Int. J. Biol. Macromol. 162 (2020) 1849-1861. https://doi.org/10.1016/j.ijbiomac.2020.08.060.

36. B. Joseph, S. Krishnan, V.K. Sagarika, A. Tharayil, N. Kalarikkal, S. Thomas, Bionanocomposites as industrial materials, current and future perspectives: a review, Emergent Materials, 3 (2020) 711-7251. https://doi.org/10.1007/s42247-020-00133-x.

37. G. Lazzara, G. Cavallaro, A. Panchal, R. Fakhrullin, A. Stavitskaya, V. Vinokurov, Y. Lvov, An assembly of organic-inorganic composites using halloysite clay nanotubes, Curr. Opin. Colloid Interface Sci. 35 (2018) 42-50. https://doi.org/10.1016/j.clay.2019.105416.

38. G. Gorrasi, V. Senatore, G. Vigliotta, S. Belviso, R. Pucciariello, PET-Halloysite nanotubes composites for packaging application: Preparation, characterization and analysis of physical properties, Eur. Polym. J. 61 (2014) 145-156. http://dx.doi.org/10.1016/j.eurpolymj.2014.10.004.

39. G. Gorrasi, R. Pantani, M. Murariu, P. Dubois, PLA/Halloysite Nanocomposite Films: Water Vapor Barrier Properties and Specific Key Characteristics, Macromol. Mater. Eng. 299 (2014) 104-115. https://doi.org/ 10.1002/mame.201200424.

40. V. Donchak, Y. Stetsyshyn, M. Bratychak, G. Broza, K. Harhay, N. Stepina, M. Kostenko, S. Voronov, 2021. Nanoarchitectonics at surfaces using multifunctional initiators of surface-initiated radical polymerization for fabrication of the nanocomposites. Appl. Surface Sci. Advances 5, 100104. https://doi.org/10.1016/j.apsadv.2021.100104.

41. S. Kalay, Y. Stetsyshyn, V. Lobaz, K. Harhay, H. Ohar, M. Çulha, 2015. Water-dispersed thermo-responsive boron nitride nanotubes: Synthesis and properties. Nanotechnology 27, 035703. https://doi.org/10.1088/0957-4484/27/3/035703.

42. S. Kalay, Y. Stetsyshyn, V. Donchak, K. Harhay, O. Lishchynskyi, H. Ohar, Y. Panchenko, S. Voronov, M. Çulha, pH-Controlled fluorescence switching in water-dispersed polymer brushes grafted to modified boron nitride nanotubes for cellular imaging, Beilstein J. Nanotechnol. 10 (2019) 2428-2439. https://doi.org/10.3762/bjnano.10.233.

43. G. Ciofani, G.G. Genchi, I. Liakos, A. Athanassiou, D. Dinucci, F. Chiellini, V. Mattoli, A simple approach to covalent functionalization of boron nitride nanotubes, J. Colloid Interface Sci. 374 (2012) 308-314. https://doi.org/10.1016/j.jcis.2012.01.049.

44. De Bin Jiang, S.Yuan, X.Cai, G. Xiang, Y. Xin Zhang, S. Pehkonen, X. Ying Liu, Magnetic nickel chrysotile nanotubes tethered with pH-sensitive poly(methacrylic acid) brushes for Cu(II) adsorption, J. Mol. Liq. 276 (2019) 611-623. https://doi.org/10.1016/j.molliq.2018.12.048.

45. Xiaowei Pei, Jingcheng Hao, Weimin Liu, Preparation and Characterization of Carbon Nanotubes-Polymer/Ag Hybrid Nanocomposites via Surface RAFT Polymerization, J. Phys. Chem. C 111 (2007) 2947-2952. https://doi.org/10.1021/jp0673213.

46. Trinh D. Nguyen, Sang T. Vo, Md R. Islam, Kwon T. Lim, Dai-Viet N. Vo, Long G. Bach, Functionalization of halloysite nanotube surfaces via controlled living radical polymerization: covalent immobilization of penicillin for a bioactive interface, J. Chem. Technol. Biotechnol. 94 (2019) 1416-1424. https://doi.org/10.1002/jctb.5888.

47. Y. Hou, J. Jiang, K. Li, Y. Zhang, J. Liu, Grafting Amphiphilic Brushes onto Halloysite Nanotubes via a Living RAFT Polymerization and Their Pickering Emulsification Behavior, J. Phys. Chem. B 118 (2014) 1962-1967. https://doi.org/10.1021/jp411610a.

48. S. Nastyshyn, J. Raczkowska, Y. Stetsyshyn, B. Orzechowska, A. Bernasik, Y. Shymborska, M. Brzychczy-Włoch, T. Gosiewski, O. Lishchynskyi, H. Ohar, D. Ochońska, K. Awsiuk, A. Budkowski, Non-cytotoxic, temperature-responsive and antibacterial POEGMA based nanocomposite coatings with silver nanoparticles, RSC Adv. 10 (2020) 10155-10166. https://doi.org/10.1039/C9RA10874B.

49. J. Raczkowska, Y. Stetsyshyn, K. Awsiuk, M. Brzychczy-Włoch, T. Gosiewski, B. Jany, O. Lishchynskyi, Y. Shymborska, S. Nastyshyn, A.Bernasik, H. Ohar, F. Krok, D. Ochońska, A. Kostruba, A. Budkowski, 2019. "Command" surfaces with thermo-switchable antibacterial activity. Mater. Sci. Eng. C Mater. Biol. Appl. 103, 109806. https://doi.org/10.1016/j.msec.2019.109806.

50. A. Weissberger, E. Proskauer, J. Riddick, E. Toups, Organic solvents, Wiley Interscience, New York, 1955.

51. N.A. Milas, D.M. Surgenor, Studies in Organic Peroxides. VIII. t-Butyl Hydroperoxide and Di-t-butyl Peroxide, J. Am. Chem. Soc. 68 (1946) 205-208. https://doi.org/10.1021/ja01206a017.

52. M. Bratychak, W. Brostow, V. Donchak, Functional peroxides and peroxy oligoesters on the basis of pyromelitic dianhydride, Mater. Res. Innovat. 5 (2002) 250-256. https://doi.org/10.1007/s10019-002-0166-6.

53. Y. Stetsyshyn, J. Zemla, O. Zolobko, K. Fornal, A. Budkowski, A. Kostruba, V. Donchak, K. Harhay, K. Awsiuk, J. Rysz, A. Bernasik, S. Voronov, Temperature and pH dual-responsive coatings of oligoperoxide-graft-poly (N-isopropylacrylamide): Wettability, morphology, and protein adsorption, J. Colloid Interface Sci. 387 (2012) 95-105. http://doi.org/10.1016/j.jcis.2012.08.007.

54. Y. Stetsyshyn, J. Raczkowska, K. Harhay, K. Gajos, Y. Melnyk, P. Dąbczyński, T. Shevtsova, A. Budkowski, Temperature-responsive and multi-responsive grafted polymer brushes with transitions based on critical solution temperature: Synthesis, properties, and applications, Colloid Polym. Sci. 299 (2020) 363-383. https://doi.org/10.1007/s00396-020-04750-0.

55. A.A. Zezin, A.A. Zharikov, A.I. Emel'yanov, A.S. Pozdnyakov, G.F. Prozorova, S.S. Abramchuk, E.A. Zezina, 2021. A one-pot preparation of metal polymer nanocomposites in ir-radiated aqueous solutions of 1-vinyl-1,2,4-triazole and silver ions. Polymers 13, 4235. https://doi.org/10.3390/polym13234235.

56. E.M. Benetti, X.F. Sui, S. Zapotoczny, G.J. Vancso, Surface-Grafted Gel-Brush/Metal Nanoparticle Hybrids, Adv. Funct. Mater. 20 (2010) 939-944. https://doi.org/10.1002/adfm.200902114.

57. W. Meng, Q. He, M. Yu, Y. Zhou, C. Wang, B. Yu, B. Zhang, W. Bu, Telechelic amphiphilic metallopolymers endfunctionalized with platinum (II) complexes: synthesis, luminescence enhancement, and their self-assembly into flowerlike vesicles and giant flowerlike vesicles, Polym. Chem. 10 (2019) 4477-4484. https://doi.org/10.1039/C9PY00652D.

58. J.M. Falcón, T. Sawczen, I.V. Aoki, 2015. Dodecylamine-loaded halloysite nanocontainers for active anticorrosion coatings. Front. Mater. 2, 69. http://dx.doi.org/10.3389/fmats.2015.00069.

59. H. Cheng, Q. Liu, J. Yang, J. Zhang, R.L. Frost, Thermal analysis and infrared emission spectroscopic study of halloysite potassium acetate intercalation compound, Thermochim. Acta. 511 (2010) 124-128. https://doi.org/10.1016/j.tca.2010.08.003.

60. M. Liu, C. Wu, Y. Jiao, S. Xiong, C. Zhou, Chitosan-halloysite nanotubes nanocomposite scaffolds for tissue engineering. J. Mater. Chem. B. 1 (2013) 2078-2089. https://doi.org/10.1039/C3TB20084A.

61. A.M. Carrillo, C.M. Urruchurto, J.G. Carriazo, S. Moreno, R.A. Molina, Structural and textural characterization of a Colombian halloysite, Rev. Mex. Ing. Quim. 13 (2014) 563-571. http://rmiq.org/ojs311/index.php/rmiq/article/view/1351.

62. K. Tasaki, Poly(oxyethylene)−water interactions: a molecular dynamics study, J. Am. Chem. Soc. 118 (1996) 8459-8469. https://doi.org/10.1021/ja951005c.

63. Z. Hu, T. Cai, C. Chi, Thermoresponsive oligo(ethylene glycol)-methacrylate- based polymers and microgels, Soft Matter. 6 (2010) 2115-2123. https://doi.org/10.1039/B921150K.

64. J.F. Lutz, Thermo-switchable materials prepared using the OEGMA-platform, Adv. Mater. 23 (2011), 2237-2243. https://doi.org/10.1002/adma.201100597.

65. K. Skrabania, J. Kristen, A. Laschewsky, Ö. Akdemir, A. Hoth, J.F. Lutz, Design, synthesis, and aqueous aggregation behavior of nonionic single and multiple thermoresponsive polymers, Langmuir 23 (2007) 84-93. https://doi.org/10.1021/la061509w.

66. Y. Stetsyshyn, K. Awsiuk, V. Kusnezh, J. Raczkowska, B.R. Jany, A. Kostruba, K. Harhay, H. Ohar, O. Lishchynskyi, Y. Shymborska, Y. Kryvenchuk, F. Krok, A. Budkowski, Shape-controlled synthesis of silver nanoparticles in temperature-responsive grafted polymer brushes for optical applications, Appl. Surf. Sci. 463 (2019) 1124-1133. http://doi.org/10.1016/j.apsusc.2018.09.033.

67. E. Saion, E. Gharibshahi, K. Naghavi, Size-Controlled and Optical Properties of Monodispersed Silver Nanoparticles Synthesized by the Radiolytic Reduction Method, Int. J. Mol. Sci. 14 (2013) 7880-7896. http://doi.org/10.3390/ijms14047880.

68. K. Anandalakshmi, J. Venugobal, V. Ramasamy, Characterization of silver nanoparticles by green synthesis method using *Pedalium murex* leaf extract and their antibacterial activity, Appl. Nanosci. 6 (2016) 399-408. https://doi.org/10.1007/s13204-015-0449-z.

69. L.A. Austin, M.A. Mackey, E.C. Dreaden, M.A. El-Sayed, The optical, photothermal, and facile surface chemical properties of gold and silver nanoparticles in biodiagnostics, therapy, and drug delivery, Arch. Toxicol. 88 (2014) 1391-1417. https://doi.org/10.1007/s00204-014-1245-3.

70. M. Yamada, M. Foote, T.W. Prow, Therapeutic gold, silver, and platinum nanoparticles, Wiley Interdiscip. Rev. Nanomed. Nanobiotechnol. 7 (2015) 428-445. https://doi.org/10.1002/wnan.1322.

71. M. He, Q. Wang, J. Zhang, W. Zhao, C. Zhao, Substrate-independent Ag-nanoparticle-loaded hydrogel coating with regenerable bactericidal and thermoresponsive antibacterial properties, ACS Appl. Mater. Interfaces 9 (2017) 44782-44791. https://doi.org/10.1021/acsami.7b13238.

72. H. Yang, G. Li, J. Stansbury, X. Zhu, X. Wang, J. Nie, Smart antibacterial surface made by photopolymerization, ACS Appl. Mater. Interfaces 8 (2016) 28047-28054. https://doi.org/10.1021/acsami.6b09343.

73. S. Konnova, A. Danilushkina, G. Fakhrullina, F. Akhatova, A. Badrutdinov, R. Fakhrullin, Silver nanoparticle-coated "cyborg" microorganisms: rapid assembly of polymer stabilized nanoparticles on microbial cells, RSC Adv. 5 (2015) 13530-13537. https://doi.org/10.1039/c4ra15857a.

74. G. Lazzara, R.F. Fakhrullin, eds., Nanotechnologies and nanomaterials for diagnostic, conservation and restoration of cultural heritage. Elsevier, 2018. https://doi.org/10.1016/C2017-0-00296-3.

75. S. Cheeseman, A.J. Christofferson, R. Kariuki, D. Cozzolino, T. Daeneke, R.J. Crawford, A. Elbourne, 2020. Antimicrobial metal nanomaterials: from passive to stimuli-activated applications. Advanced Sci. 7, 1902913. https://doi.org/10.1002/advs.201902913.

76. M. Licchelli, M. Malagodi, M. Weththimuni, C. Zanchi, Nanoparticles for conservation of bio-calcarenite stone, Applied Physics A 114 (2014) 673-683. http://dx.doi.org/10.1007/s00339-013-7973-z.

77. Y. Ocak, A. Sofuoglu, F. Tihminlioglu, H. Böke, Sustainable bio-nano composite coatings for the protection of marble surfaces, J. Cult. Herit. 16 (2015) 299-306. https://doi.org/10.1016/j.culher.2014.07.004.

78. G. Cavallaro, G. Lazzara, S. Konnova, R. Fakhrullin, Y. Lvov, Composite films of natural clay nanotubes with cellulose and chitosan, Green Materials 2 (2014) 232-242. https://doi.org/10.1680/gmat.14.00014.

79. S. Spile, T. Suzuki, J. Bendix, K.P. Simonsen, 2016. Effective cleaning of rust stained marble. Heritage Sci. 4, 12. https://doi.org/10.1186/s40494-016-0081-6.

80. I. Armentano, M. Barbanera, E. Carota, S. Crognale, M. Marconi, S. Rossi, G. Rubino, M. Scungio, J. Taborri, G. Calabrò, Polymer Materials for Respiratory Protection: Processing, End Use, and Testing Methods, ACS Appl. Polym. Mater. 3 (2021) 531-548. https://doi.org/10.1021/acsapm.0c01151.

81. C. Balagna, S. Perero, E. Percivalle, E.V. Nepita, M. Ferraris, 2020. Virucidal Effect against Coronavirus SARS-CoV-2 of a Silver Nanocluster/Silica Composite Sputtered Coating. Open Ceramics 1, 100006. https://doi.org/10.1016/j.oceram.2020.100006.

82. S.R. Safi, T. Nakata, S. Hara, T. Gotoh, T. Iizawa, S. Nakai, 2020. Synthesis, Phase-Transition Behaviour, and Oil Adsorption Performance of Porous Poly(oligo(ethylene glycol) Alkyl Ether Acrylate) Gels. Polymers 12, 1405. https://doi.org/10.3390/polym12061405.

83. A. D'Agostino, A. Taglietti, R. Desando, M. Bini, M. Patrini, G. Dacarro, L. Cucca, P. Pallavicini, P. Grisoli, 2017. Bulk Surfaces Coated with Triangular Silver Nanoplates: Antibacterial Action Based on Silver Release and Photo-Thermal Effect. Nanomaterials (Basel) 7, 7. https://dx.doi.org/10.3390%2Fnano7010007.

84. A. D'Agostino, A. Taglietti, P. Grisoli, G. Dacarro, L. Cucca, M. Patrini, P. Pallavicini, Seed mediated growth of silver nanoplates on glass: exploiting the bimodal antibacterial effect by near IR photo-thermal action and Ag^{+} release, RSC Adv. 6 (2016) 70414-70423. https://doi.org/10.1039/C6RA11608F.

85. A. Kleinauskas, S. Rocha, S. Sahu, Y.P. Sun, P. Juzenas, 2013. Carbon-core silver-shell nanodots as sensitizers for phototherapy and radiotherapy. Nanotechnology 24, 325103. https://doi.org/10.1088/0957-4484/24/32/325103.